Validation of an Instability Growth Model Using Particle Image Velocimetry Measurements

K. Prestridge,[1] P. Vorobieff,[2] P. M. Rightley,[1] and R. F. Benjamin[1]

[1]*Dynamic Experimentation Division, Los Alamos National Laboratory, Los Alamos, New Mexico 87545*
[2]*Department of Mechanical Engineering, University of New Mexico, Albuquerque, New Mexico 87131*

(Received 2 December 1999)

A varicose-profile, thin layer of heavy gas (SF_6) in lighter gas (air) is impulsively accelerated by a planar, Mach 1.2 shock, producing the Richtmyer-Meshkov instability. We present the first measurements of the circulation in the curtain during the vortex-dominated, nonlinear stage of the instability evolution. These measurements, based on particle image velocimetry data, are employed to validate an idealized model of the nonlinear perturbation growth.

PACS numbers: 47.20.Ma, 47.20.Ky, 47.40.Nm

In this study, we present experimental measurements of the circulation in a shock-accelerated thin layer of SF_6 gas embedded in air (i.e., gas curtain). With these measurements, we validate an inviscid, point-vortex model of nonlinear gas-curtain instability growth [1] by comparing our results with its predicted parameter, the circulation of the vortex cores. This is the first time that the circulation derived from a simple model of mixing width growth has been compared to a measured value of circulation. This comparison provides the connection among an inviscid model, traditional integral measurements of the mixing-layer width, and detailed velocity-field measurements.

Instabilities of accelerated interfaces between fluids of different densities exist in a vast range of processes—from shaking sauce out of a bottle [2] to supernova explosions [3]. Richtmyer-Meshkov instability (RMI) is the impulsively accelerated analog of Rayleigh-Taylor instability. RMI has attracted considerable recent attention because of its practical importance for inertial confinement fusion [4], where the mixing associated with RMI can cause contamination of the fuel and also distort the converging shell, rendering compression less effective. RMI is also an effective test problem for hydrodynamic instability and transition to turbulence studies [5,6], and as a benchmark for code validation [7,8]. This instability is an open flow problem, of which there are far fewer good examples than for closed systems.

RMI developing on shock-accelerated, perturbed density interfaces goes through several stages of evolution before eventual transition to turbulence [9]. The initial, linear growth stage was first theoretically described by Richtmyer [10]. Subsequently, the instability grows in a nonlinear manner, and the flow is dominated by the vortices created by the initial baroclinic vorticity generation. Several theoretical models have been developed to describe this nonlinear region of the instability's development [1,11–14]. Only measurements of large-scale features of the flow have been available to validate those growth models up to now. While our present findings describe the second stage of the curtain evolution (nonlinear, vortex-dominated growth), the same experimental technique applied at later times can produce quantitative information about the transition to turbulence.

We study the development of the interfaces of a perturbed curtain (i.e., thin layer) of heavy gas (SF_6) embedded in ambient air when the curtain is accelerated by a Mach 1.2 normal shock created in a horizontal shock tube. The shock-tube facility is the same as that used in earlier experiments [15–17], except for the improved diagnostics. The current experimental configuration will be described in detail elsewhere [18].

The test section of the shock tube (75 mm square) is shown in Fig. 1. A laminar curtain of SF_6 is injected through a contoured nozzle vertically into the top side of the test section and removed on the bottom side. The nozzle profile imposes a varicose perturbation with dominant wavelength $\lambda = 6$ mm on the curtain. The SF_6 is seeded with small ($d \leq 0.5$ μm) glycol/water droplets from a theatrical fog generator which allow us to make the particle image velocimetry (PIV) measurements. See Refs. [9] and [18] for detailed analyses which show that the fog particles

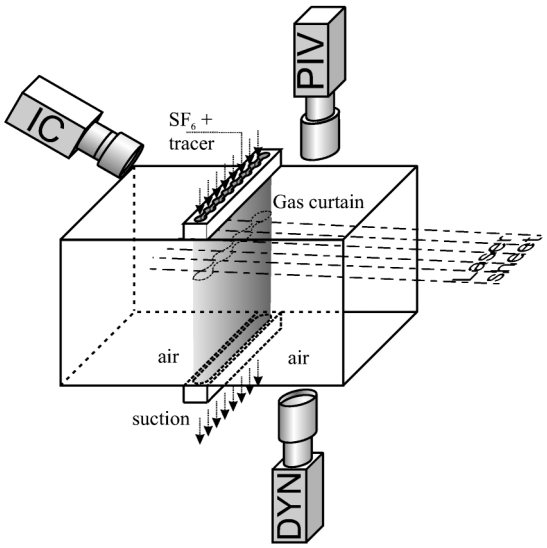

FIG. 1. Shock-tube test section (shock propagates from left to right).

accurately track the SF_6 curtain. The tube creates high quality planar shocks of Mach 1.2 that propagate through the test section and accelerate the curtain.

The gas curtain is illuminated using two frequency-doubled, pulsed Nd:YAG lasers, the first of which is a customized, burst-mode laser that is configured to fire seven pulses (100-ns duration, 3 mJ) spaced 140 μs apart. The second is a commercial 10 Hz laser with a 10-ns, 10-mJ pulse, which is fired once per event. The light from both lasers is focused into coplanar, horizontal sheets in the test section, as shown in Fig. 1, and three single-frame, gated, intensified CCD cameras (1134 $\times$ 468 pixels) look at fixed, preset fields of view. The "IC" camera records the image of the initial conditions on one frame, while the "Dynamic" ("DYN" in Fig. 1) camera observes the rest of the test section to capture multiple exposures of the gas curtain as it is advected downstream. The large free stream velocity causes all of the images to be physically separated on the CCD. The "PIV" camera focuses on a small region of the dynamic field, about 19 by 14 mm, to detect the individual fog droplets.

An image with the view of the initial conditions and the dynamic image from the IC and Dynamic cameras are shown in Fig. 2. The actual image from the PIV camera is double exposed, first from the burst-mode laser at 675 μs, and then from the single-pulse laser at 693.4 μs. The latter is not recorded by the Dynamic camera because the camera intensifier is gated off during the second pulse.

The negative of the image captured by the PIV camera is shown in Fig. 3a. Visible in the figure is the double exposure caused by the two different laser pulses, separated by 18.4 μs. Also labeled in the figure are two large-scale features of the flow, mushrooms A and B. We will use these features to illustrate the process of determining mixing width and circulation in the flow field. Figure 3b is the velocity field created by performing single-frame cross correlation on the image in Fig. 3a. We take the velocity field to be representative of a time midway between the two exposures of Fig. 3a, at 684.2 μs after shock impact. The measured free stream velocity of 97 m/s has been subtracted from the field. The blank regions correspond to areas with tracer seeding insufficient for reliable cross-correlation analysis [18].

From this velocity field, a vorticity field is created by calculating the circulation around each vector using the eight surrounding vectors [19]; this is shown in Fig. 3c. What becomes apparent is that each roll-up region at the intersection of the mushroom "stem" and "cap" in Fig. 3a corresponds to a concentration of vorticity, and there is a pair of counterrotating vortices matching each mushroom. We expect this from observations of the image, and it is confirmed by the PIV measurements.

Using this new flow-field information contained within the large-scale structures, we can now compare the circulation determined from an inviscid growth model with that measured using PIV. Let us first briefly summarize the

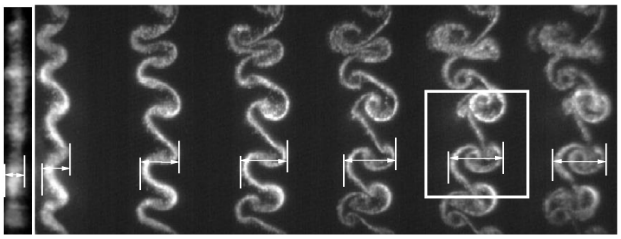

FIG. 2. Initial conditions ($t = 0$) and dynamic images at $t =$ 115, 255, 395, 535, 675, and 815 μs after shock interaction. Region imaged by the PIV camera is inside the white rectangle. Also indicated are regions where curtain width was measured for one wavelength.

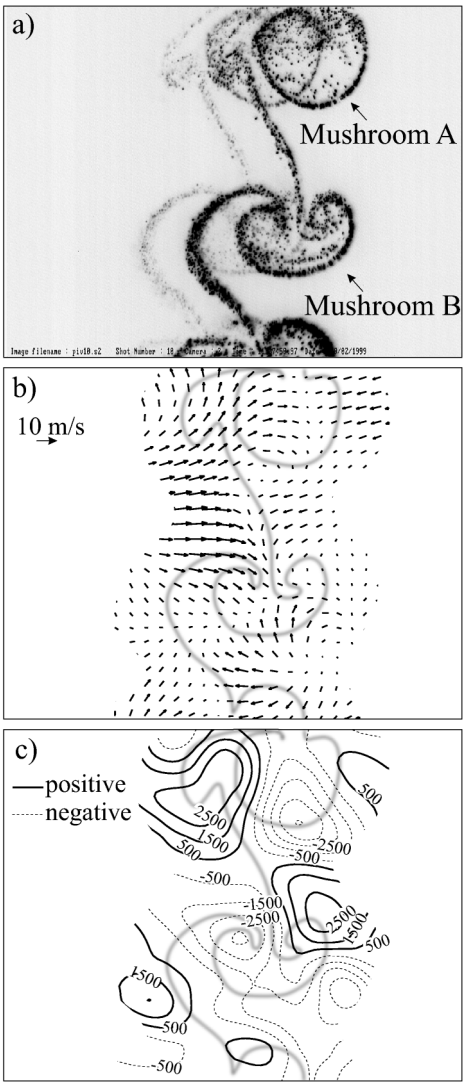

FIG. 3. PIV measurements. (a) Region captured by the PIV camera with two prominent mushroom structures labeled. (b) Velocity field corresponding to the image (a). (c) Vorticity isocontours, in s^{-1}. The gray lines in (b) and (c) show the position of the curtain midway between the two exposures of (a).

important features of the model for the growth of the mixing region [1,17].

The model is based upon an infinite row of counterrotating point vortices, approximating the vorticity which is baroclinically generated on the interfaces between the heavy and light gases when the shock impacts the curtain. Each vortex has the same circulation, Γ, and there is one local wave number associated with the flow, k, where $k = 2\pi/\lambda$. For the single-mode nozzle used in these experiments, $\lambda = 6$ mm, and k was set at a fixed value of 1.04 mm^{-1}. The expression for the growth of the mixing region in time is [1,17]:

$$w(t) = \frac{2}{k}\sinh^{-1}\left[k^2\Gamma(t - t_0) + \sinh\left(\frac{kw_0}{2}\right)\right], \quad (1)$$

where t_0 is the virtual origin and w_0 is the curtain width just after it has been compressed by the shock. This value is estimated to be $w_0 = w_{\text{init}}/1.34$, where the measured thickness is divided by the shock compression factor for a Mach 1.2 normal shock. The virtual origin t_0, absent from the original model [1], is introduced to account for the phase inversion of one of the interfaces [17,20]. Equation (1) produces a growth rate prediction similar to other nonlinear-growth theories [13,14].

Previous analysis quantified the initial thickness and temporal growth of the layer [17], but the actual circulation of the flow could not be measured. We will continue with the example of Figs. 2 and 3, and illustrate how we measure the growth of the mixing region in the gas curtain. Figure 2 shows how the mixing width is measured for mushroom B, as indicated by the white lines on the image. To preserve the local flow information, we measured the individual widths corresponding to the wavelengths along which each mushroom appeared.

The mixing width evolutions from Fig. 2 for mushrooms A and B are plotted in Fig. 4. It is immediately apparent that the mixing widths corresponding to each mushroom are very similar. Using Γ and t_0 as free parameters, where w_0 and k are fixed parameters measured from the initial conditions, the $w(t)$ data are fit to Eq. (1) (these fits are also shown in Fig. 4). The value k remains nearly constant during instability growth, even though mushroom orientation varies. The model from Eq. (1) converges with residuals, r^2, of 0.975 and 0.955, respectively, where $r^2 = 1.0 - \sum_{i=1}^{n}[(w_{\text{fit}} - w_i)^2/(w_i - \bar{w})^2]$ and $\bar{w}$ is the average width of the curtain. Each curve fit gives us a different circulation for the corresponding mushroom, such that $\Gamma_{\text{curve fit-A}} = 0.039$ $\text{mm}^2/\mu\text{s}$ and $\Gamma_{\text{curve fit-B}} = 0.046$ $\text{mm}^2/\mu\text{s}$.

We also applied the method for computing circulation based upon another idealized model [1]. In that model, the counterrotating vortices roll up from vortex sheets formed on the density interfaces (assumed sharp) after the impulsive acceleration ΔV. The strength of an individual vortex for a varicose layer with initial perturbation amplitude a_0 and wave number k is [1]:

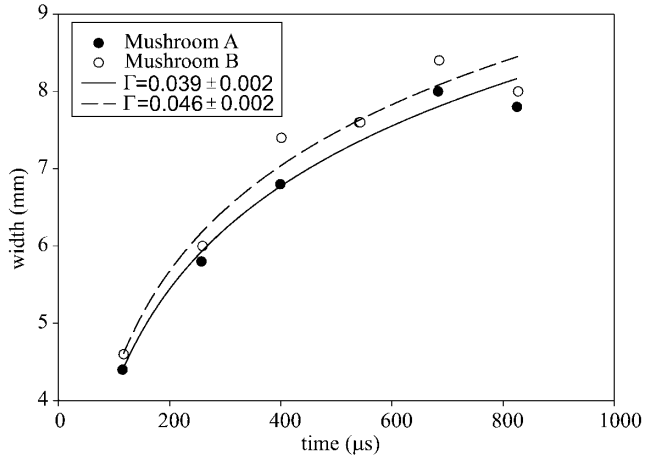

FIG. 4. Curve fits using the growth model in Eq. (1) for mushrooms A and B of Fig. 3a. Symbols are experimental data; lines are curve fits. Error bars on data points are no larger than the points.

$$\Gamma = -\frac{2}{\pi}\frac{(\rho_2 - \rho_1)[1 + \tanh(kw_0/2)]\Delta V a_0}{\rho_2 \tanh(kw_0/2) + \rho_1}, \quad (2)$$

with densities ρ_1 (light) and ρ_2 (heavy). For our flow, $\Delta V = 100$ m/s, $w_0 = 2.2$ mm, and $a_0 = 0.45$ mm, resulting in Eq. (2) yielding $\Gamma = 0.04$ $\text{mm}^2/\mu\text{s}$—consistent with the curve-fit results of 0.039 and 0.046 $\text{mm}^2/\mu\text{s}$.

To validate the model in Eq. (1), we compare the circulations from the curve fits of Fig. 4 to the vorticity field of Fig. 3c. The circulation from the PIV data was calculated by drawing a closed curve around each region of negative vorticity and computing the line integral of tangential velocity around the entire curve. This process yields circulations: $\Gamma_{\text{PIV-A}} = 0.041$ $\text{mm}^2/\mu\text{s}$ and $\Gamma_{\text{PIV-B}} = 0.033$ $\text{mm}^2/\mu\text{s}$. We measured Γ with the curve-fitting and PIV procedures for other data sets, and the comparison between Γ_{PIV} and $\Gamma_{\text{curve fit}}$ is shown in Fig. 5. The range of circulation values from 0.01 to 0.11 $\text{mm}^2/\mu\text{s}$ is caused by uncontrolled but carefully measured variations in the initial state of the varicose interface. The agreement shown in Fig. 5 is quite good, with over two-thirds of the data within an error bar of the fit, $\Gamma_{\text{PIV}} = \Gamma_{\text{curve fit}}$. Thus, the model [Eq. (1)] is a reliable estimator of mixing width during this phase of the instability. It is also noteworthy that the delay, t_0, recovered by the curve fit varied from 0 to 60 μs, which is consistent with the duration of the phase inversion observed in our experiments [21].

Several physical effects contribute to observed differences. The model assumes an initially sharp interface, but the actual interface is diffuse [17,18]. Also, mode coupling, not included in the model, is beginning at the time of the PIV measurements. For several events in Fig. 5 the counterrotating vortices are not perfectly aligned in the spanwise direction, as assumed by the model. The correlation of Γ values shown in Fig. 5 is quite good despite these limitations, which suggests that the inviscid vortex

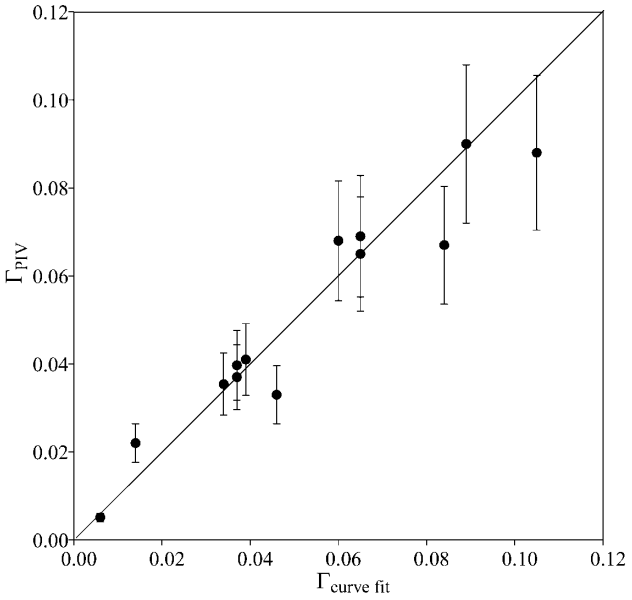

FIG. 5. Comparison between the circulation measured using PIV and the circulation from the curve fits of Eq. (1) of mixing width growth for many experiments similar to the one in Fig. 3. Error bars represent PIV measurement uncertainty.

dynamics driving the instability are fairly robust, and that dissipation is negligible.

In summary, we have shown that there is agreement between the circulations determined directly from PIV measurements and the circulations deduced from curve fits of the model represented by Eq. (1) to measured mixing width data. Thus, the growth of the curtain with a single, dominant wavelength during the period of nonlinear, vortex-dominated evolution can be modeled using inviscid mechanisms in the regime which we have examined ($t < 1$ ms). Under these flow conditions, there is little apparent dissipation of the initial vorticity deposited in the gas curtain by the shock, as indicated by the close match between the circulation of the idealized model and the circulation calculated from the velocity-field measurements. For the first time, we have been able to make a strong correlation between the circulation predicted from integral measurements of the mix layer and the actual circulation of the large-scale vortex structures within the layer.

This work was supported by the DOE Contract No. W-7405-ENG-36 and by Sandia National Laboratories Grant No. BG-7553. We would like to acknowledge the technical assistance of Norman Kurnit and the continuing support of Jas Mercer-Smith and Phil Goldstone.

[1] J. W. Jacobs *et al.,* J. Fluid Mech. **295,** 23 (1995).
[2] R. F. Benjamin, The Phys. Teacher **37,** 332 (1999).
[3] A. Burrows, J. Hayes, and B. A. Fryxell, Astrophys. J. **450,** 830 (1995).
[4] R. J. Taylor *et al.,* Phys. Rev. Lett. **79,** 1861 (1997).
[5] P. Vorobieff, P. M. Rightley, and R. F. Benjamin, Phys. Rev. Lett. **81,** 2240 (1998).
[6] P. Vorobieff, P. M. Rightley, and R. F. Benjamin, Physica (Amsterdam) **133D,** 469 (1999).
[7] R. M. Baltrusaitis *et al.,* Phys. Fluids **8,** 2471 (1996).
[8] R. L. Holmes *et al.,* J. Fluid Mech. **389,** 55 (1999).
[9] P. M. Rightley *et al.,* Phys. Fluids **11,** 186 (1999).
[10] R. D. Richtmyer, Commun. Pure Appl. Math. **23,** 297 (1960).
[11] R. Samtaney and N. Zabusky, J. Fluid Mech. **269,** 45 (1994).
[12] J. Hecht, U. Alon, and D. Shvarts, Phys. Fluids **6,** 4019 (1994).
[13] T. A. Peyser *et al.,* Phys. Rev. Lett. **75,** 2332 (1995).
[14] Q. Zhang and S. Sohn, Phys. Fluids **9,** 1106 (1997).
[15] J. W. Jacobs *et al.,* Phys. Rev. Lett. **70,** 583 (1993).
[16] J. M. Budzinski, R. F. Benjamin, and J. W. Jacobs, Phys. Fluids **6,** 3510 (1994).
[17] P. M. Rightley, P. Vorobieff, and R. F. Benjamin, Phys. Fluids **9,** 1770 (1997).
[18] K. Prestridge *et al.* (to be published).
[19] *VISIFLOW System User Manual* (AEA Technology, Oxfordshire, UK, 1997).
[20] Y. Yang, Q. Zhang, and D. H. Sharp, Phys. Fluids **6,** 1856 (1994).
[21] P. Vorobieff, P. M. Rightley, and R. F. Benjamin, in Proceedings of the 6th IWPCTM Workshop, Marseilles, 1997 (to be published).